V European Conference on Computational Fluid Dynamics
ECCOMAS CFD 2010
J. C. F. Pereira and A. Sequeira (Eds)
Lisbon, Portugal,14-17 June 2010

ENDOTHELIAL SHEAR STRESS FROM LARGE-SCALE BLOOD FLOW SIMULATIONS

S. Melchionna[*], J. Lätt[*], E. Kaxiras[*], A. Peters[†], M. Bernaschi[††], S. Succi[††]

[*]Institute of Materials Science and Engineering
École Polytechnique Fédérale de Lausanne, Switzerland
[†]Department of Physics and School of Engineering and Applied Sciences,
Harvard University, Cambridge, MA, USA
[††]Istituto Applicazioni Calcolo,
Consiglio Nazionale delle Ricerche, Rome, Italy

Key words: Lattice Boltzmann, hemodynamics, endothelial shear stress

Abstract. *We discuss the optimal evaluation of endothelial shear stress for real-life case studies based on anatomic data acquisition. The fluid dynamic simulations require smoothing of the geometric dataset to avoid major artifacts in the flow patterns. We discuss the evaluation of the endothelial shear stress at different levels of smoothness and the conditions to obtain satisfactory convergence at increasing smoothness.*

1 INTRODUCTION

Atherosclerosis is the most common cardiovascular disease and responsible for $\sim 35\%$ of annual deaths in developed countries [1]. Although the development of atherosclerosis depends on the presence of systemic risk factors, the disease results from the accumulation of lipid molecules within the wall of the blood vessels, as well as from enhanced exposure to intramural penetration of nano-sized biological bodies, such as B-cells. Atherosclerotic plaques appear in regions of disturbed blood flow where the local endothelial shear stress (ESS) is low (< 1.0 Pa) or of alternating direction [2] and tend to form near arterial branches and bifurcations where the flow is always disturbed as compared to un-branched regions [3, 4].

Atherosclerosis primarily affects the arterial coronary arteries. Predictions of where and how the disease is likely to develop can be obtained by fluid-dynamics simulations as a routine methodology to study blood flow patterns in human coronary arteries. A direct benefit of the simulation approach is to understand the connection between fluid-mechanical flow patterns and plaque formation and evolution, with important implications for predicting the course of atherosclerosis and possibly preventing or mitigating its effects.

The joint use of simulation and imaging techniques allows to non-invasively screen large numbers of patients for incipient coronary disease. One option is to obtain the coronary artery wall, plaque morphology and lumen anatomy from the non-invasive Multi-Detector Computed Tomography (MDCT) imaging technique. In particular, the newest MDCT systems with 320-detector rows [5, 6] enable 3D acquistion of the entire coronary arterial tree in a single heart beat and high accuracy of nominal resolution of 0.1 mm. In spite of recent technological progress, this resolution is still insufficient and the inherently noisy geometrical data pose a problem in the evaluation of ESS, a quantity that proves extremely sensitive to the details of the wall morphology.

2 LATTICE BOLTZMANN METHOD FOR HEMODYNAMICS

Our simulations of blood flows are based on the acquisition of MDCT data which are segmented into a stack of slices, followed by a mesh generation from the segmented slices. For a typical coronary artery system, the procedure to build the LB mesh from the MDCT raw data starts from a single vessel, formatted as stacked bi-dimensional contours (slices), with a nominal resolution of 0.1 mm. The contour path of each slice is irregular and shaped as a collection of 256 points. The slices are quasi-parallel and mostly transverse to the path connecting different centerlines. Moreover, the sequence of contour points is mostly aligned along the stacking sequence, that is, the contour index does not present any major twisting when moving between contiguous centerlines. Data relative to each vessel in a multi-branched geometry have the same format.

Raw MDCT data present a mild level of geometric irregularities that can affect the quality of the LB simulations. One possibility is to regularize the initial geometry by smoothing the sequence of surface points via a linear filter along the longitudinal direction.

Similarly, one could filter out surface points along the azimuthal contour. In the sequel, in order to keep the external intervention minimal, we shall focus on the longitudinal smoothing procedure only, and discuss its effects on the fluid dynamic results, as compared to the original, unsmoothed data set.

The Lattice Boltzmann (LB) method is a hydrokinetic approach to tackle complex fluid dynamic problems as in multi-branched hemodynamic simulations. Owing to its flexibility, LB is a competitive computational alternative to the discretization of the Navier-Stokes equations of continuum mechanics. In essence, LB is a minimal form of the Boltzmann kinetic equation, based on the collective dynamics of fictitious particles on the nodes of a regular lattice [7] where the basic quantity is $f_i(\vec{x},t)$, representing the probability of finding a "fluid particle" at the mesh location $\vec{x}$ and at time t and travelling with discrete speed $\vec{c}_i$. "Fluid particles" represent the collective motion of a group of physical particles (often referred to as populations).

For the LB simullations we use the MUPHY software [8], developed in our group for multiscale simulations of blood flows. We employ the common three-dimensional 19-speed cubic lattice (D3Q19) and mesh spacing Δx and where the discrete velocities $\vec{c}_i$ connect mesh points to first and second neighbors [9]. The fluid populations are advanced in a timestep Δt through the following evolution equation

$$f_i(\vec{x}+\vec{c}_i\Delta t, t+\Delta t) = f_i(\vec{x},t) - \omega\Delta t(f_i - f_i^{eq})(\vec{x},t) \tag{1}$$

The right hand side of Eq. (1) represents the effect of fluid-fluid molecular collisions, through a relaxation towards a local equilibrium, f_i^{eq}, typically a second-order expansion in the fluid velocity of a local Maxwellian with speed $\vec{u}$,

$$f_i^{eq} = w_i\rho\left[1 + \frac{\vec{u}\cdot\vec{c}_i}{c_s^2} + \frac{\vec{u}\vec{u}:(\vec{c}_i\vec{c}_i - c_s^2\overleftrightarrow{I})}{2c_s^4}\right] \tag{2}$$

where $c_s = 1/\sqrt{3}$ is the speed of sound, w_i is a set of weights normalized to unity, and $\overleftrightarrow{I}$ is the unit tensor in Cartesian space. The relaxation frequency ω controls the kinematic viscosity of the fluid, $\nu = c_s^2\Delta t\left(\frac{1}{\omega} - \frac{1}{2}\right)$. The kinetic moments of the discrete populations f_i provide the local mass density $\rho(\vec{x},t) = \sum_i f_i(\vec{x},t)$ and mass current $\rho\vec{u}(\vec{x},t) = \sum_i \vec{c}_i f_i(\vec{x},t)$.

The LB is a low-Mach, weakly-compressible fluid solver and presents several major advantages for the practical implementation in complex geometries over conventional Navier-Stokes solvers. In particular, in hemodynamic simulations, the curved blood vessels are shaped on the LB Cartesian mesh scheme via a staircase representation, in contrast to body-fitted grids that can be employed in direct Navier-Stokes simulations. This apparently crude representation of the vessel walls can be systematically improved by increasing the mesh resolution. In addition, at the high mesh resolution required to sample low-noise ESS data, the LB method requires rather small time steps (of the order of 10^{-6} s for a resolution of 20 μm).

The wall shear stress, which is central to hemodynamic applications, can be computed via the shear tensor $\overleftrightarrow{\sigma}(\vec{x},t) \equiv \nu\rho\left(\vec{\partial}_x\vec{u} + \vec{\partial}_x\vec{u}^T\right)$ evaluated via its kinetic representation

$$\overleftrightarrow{\sigma}(\vec{x},t) = \frac{\nu\omega}{c_S^2}\sum_i \vec{c}_i\vec{c}_i(f_i - f_i^{eq})(\vec{x},t) \tag{3}$$

The tensor second invariant is the Endothelial Shear Stress or ESS,

$$\mathcal{S}(\vec{x}_w,t) = \sqrt{(\overleftrightarrow{\sigma} : \overleftrightarrow{\sigma})(\vec{x}_w,t)} \tag{4}$$

where $\vec{x}_w$ represents the position of sampling points in close proximity to the mesh wall nodes. $\mathcal{S}(\vec{x}_w,t)$ provides a direct measure of the strength of the near-wall shear stress [10]. It is worth mentioning that the ESS evaluation via Eq. (3), which is completely local and does not require any finite-differencing procedure, is particularly advantageous near boundaries where the computation of gradients is very sensitive to morphological details and accuracy.

An important point with regard to the choice of the sampling points $\vec{x}_w$ used to compute the ESS is the following: we take these points to coincide with the smoothed, off-lattice points forming the slice contours. Each contour point is surrounded by a small number of fluid nodes and a linear extrapolation scheme is used to evaluate the ESS. Clearly, the $\vec{x}_w$ points fall between the external fluid and wall mesh nodes and, as the mesh resolution increases, the set converges towards the exact no-slip hydrodynamic surface.

As a popular choice for imposing no-slip boundary conditions at the wall, we employ the bounce-back method; this consists of reversing at every time step the post-collisional populations pointing towards a wall node, providing first-order accuracy for irregular walls [7]. This method has extreme simplicity in handling irregular vessel boundaries, although more sophisticated alternatives are available [11, 12, 13]. In the bounce back method the points corresponding to the exact no-slip hydrodynamic surface fall at intermediate positions between the external fluid mesh nodes and the nearby wall mesh nodes.

A constant velocity (a so-called plug profile) is imposed at the entrance of the main artery, as a way to control the amplitude of the flow. This profile is not strictly speaking physically valid, because in practice the velocity drops to zero with a parabolic profile close to the wall. However, the plug profile fulfills its purpose of imposing the total flow at a chosen value. The fluid spontaneously reaches the expected parabolic profile already at a short distance after the inlet. A constant pressure is imposed on the outlet of the main artery, as well as on the outlet of all secondary branches. This leaves the simulation with the liberty of creating an appropriate velocity profile in the outlet regions, and building up a pressure drop between the inlet and the outlets.

A Zou/He boundary condition [14] is used to implement both the velocity inlet and the pressure outlets. This boundary condition exploits information streamed from fluid bulk nodes onto boundary cells, and proposes a completion scheme for particle populations

which are unknown because their neighboring nodes are not part of the fluid domain. After this, the boundary cells are treated like normal fluid cells where to execute the conventional LB scheme. Thanks to this natural integration of the boundary scheme, it can be shown theoretically that the boundary condition is implemented with second-order accuracy in space, compatible with the overall accuracy of the LB method (see [15]).

3 RESULTS

We have investigated a smooth human coronary artery system composed of a left main/LAD vessel branching into three primary vessels, labelled as LM/LAD, LCX and D1, and eight minor vessels. LM/LAD represents the longest vessel, named LM in the proximal region and LAD after the bifurcation with LCX. Overall, the test case is composed of eleven vessels, that is, one inlet vessel at the LAD level and ten outlets for all terminals. We have considered a mesh resolution of 0.05 mm corresponding to ~ 18 million voxels. At this resolution, the staircase approximation does not introduce major artifacts in the wall geometry, as analyzed in our previous publication [**?**]. In fact, the asperities in the vessel wall due to the staircase approximation account for $\lessapprox 5\%$ of the vessel diameter, while those present in the original imaging data can be as large as 50%. More importantly, our previous study has demostrated convergence of the flow profiles and ESS maps at this resolution.

In the following, we compare three different degrees of smoothness. The first is the original data set obtained directly from the imaging procedure (level-0 smoothing). The second is obtained by smoothing the geometry with a linear filter including 2 slices as left and 2 as right neighbors of each slice (level-2 smoothing). The third is obtained by smoothing via 3 slices as left and 3 as right neighbors (level-3 smoothing).

The effect of the wall smoothness is first inspected by looking at the sectional area and the volumetric flow profile along the full arterial system. In Fig. 1A and 1B we report the two profiles for the most representative vessel, the LM/LAD. Interestingly, the sectional area does not show large differences between the three data sets, only the higher level of noise is well visible. Given the above, we expect to observe roughly the same flow profile for the three cases. However, the flow profiles show marked differences between the unsmoothed and smoothed geometries. Due to mass conservation, the volumetric flow profile is quasi uniform away from bifurcations, while a drop in value corresponds to bifurcations. The flow profiles show large non-systematic differences as the vessel bifurcates. The level-0 profile has a larger pressure drop between the inlet (left-most part of the profile) and outlet (right-most part).

We expect that the wall smoothness is going to have major effects in the ESS profile since this quantity is proportional to the gradient of the velocity field and is significantly more sensitive to resolution than basic hydrodynamic fields. Moreover, ESS is proportional to the fluid dissipation due to the fluid-wall contacts. The convergence of the flow profiles to a common profile is visible in the level-2 and level-3 smoothing procedures. This is confirmed by the contour-averaged ESS, shown in Fig. 1C) for the LM/LAD

vessel and 1D) for the LCX vessel. Again, the unsmoothed geometry shows dramatic departures from the smoothed ones.

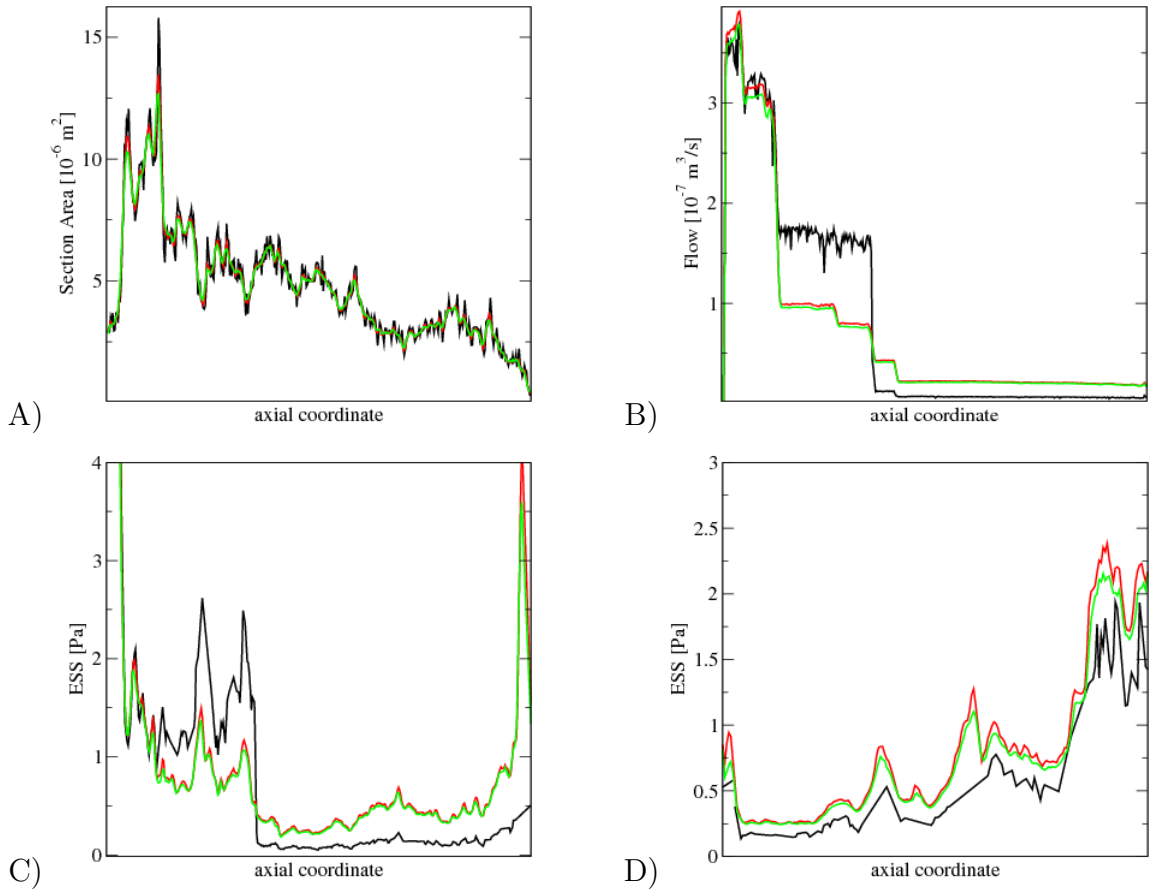

Figure 1: Hydrodynamic profiles along the vessels axial coordinate for the LM/LAD vessel for level-0 (black lines), level-2 (red lines) and level-3 (green lines) smoothing methods. A) Sectional area, B) volumetric flow-rate profile, C) contour-averaged ESS, D) contour-averaged ESS for the LCX vessel.

By looking at volumetric and contour-averaged quantities, we conclude that our smoothing procedure provides reliable geometries for stationary flows. The complete superficial distribution of ESS, however, may still exhibit strong differences at various degrees of smoothness. This is a crucial test, since the capability of simulations to predict regions prone to atherogenesis relies on the quality of the computed ESS data. The simulatioin results again show strong differences between the unsmoothed and smoothed versions, while the comparison of the two smoothed geometries shows a small dispersion in ESS. A closer visual inspection confirms this result, in particular in proximity of bifurcations and stenosis. Summarizing, once a sufficient smoothing is attained, the fine details of the ESS map show good convergence, rendering the method usable for quantitative analysis.

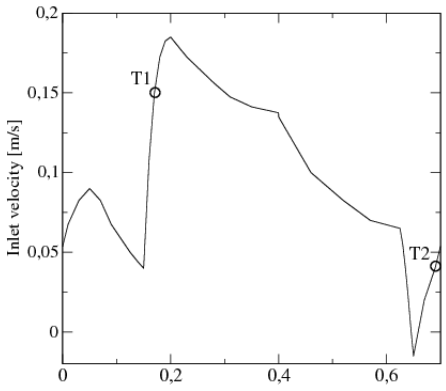

Figure 2: Inlet velocity for the pulsatile case. The labels "T1" and "T2" mark the two instants used to analyze the flow profiles and ESS maps at different degrees of smoothness.

We have next analyzed the case of a pulsatile flow. The analysis of pulsatile hemodynamics requires the investigation of the flow pattern in the time domain. Pulsatile flow is simulated by employing a time-dependent influx derived from physiological data [16]. At the inlet, the time dependent signal is shown in Fig. 3, while at the outlets we retain the constant pressure condition. We consider two representative time instants T1 and T2 and compare the flow profiles and the ESS distributions. These instants correspond to maximum Reynolds numbers of 200 and 75 at times T1 and T2, respectively. At both times, the flow profiles in Fig. 3 display similar features for the stationary flow, with a good convergence of profiles for the level-2 and level-3 degrees of smoothness.

The ESS data show that the unsmoothed geometry has a corrugated landscape, indicative of increased fluid-wall contacts. Interestingly, for this vessel the higher corrugation does not correspond to larger dissipation, that is, systematically larger ESS values. Overall, the ESS map bears a qualitative resemblance with the one of the smoothed geometry, while a more insightful analysis of putative plaque forming regions requires the use of the smoothed geometry.

In conclusion, the simulation of large-scale arterial systems relies on sophisticated imaging techniques and image reconstruction procedures. The imaging data from Multi-Detector Computed Tomography are acquired and converted into geometrical data at 0.1 mm nominal resolution. The geometry is intrinsically noisy and of little use in the direct fluid dynamic simulation of blood flow. Therefore, a smoothing procedure is needed in order to eliminate spurious corrugations in the vessel walls. This preliminary step is required to construct the cartesian mesh needed for Lattice Boltzmann simulations. We have shown that flow profiles and endothelial shear stress distributions contain major artifacts if the original geometry is not properly smoothed. Once the wall corrugations have

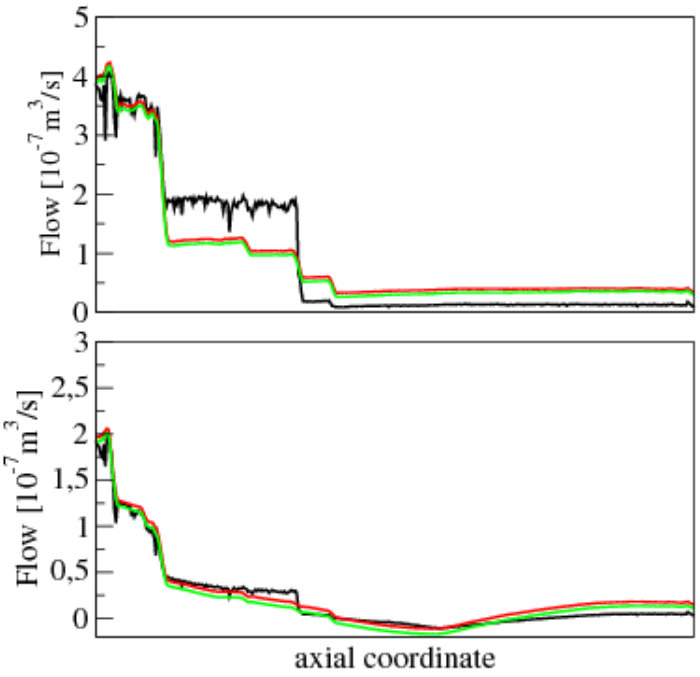

Figure 3: Pulsatile flow profiles for the LAD vessel and computed for the T1 (upper panel) and T2 (lower panel) time instants.

been filtered out, the flow patterns show profiles that are converged and insensitive to further smoothing of the surface. In essence, the Lattice Boltzmann methodology provides a reliable and robust approach to the study and understanding of cardiovascular disease in large-scale coronary arterial systems, with great potential for impact on biophysical and biomedical applications.

This work was supported by Initiative in Innovative Computing at Harvard. We wish to thank Michelle Borkin, Charles Feldman, Umit Coskun for useful discussions.

REFERENCES

[1] Heart and stroke encyclopedia, 2009, american heart association, http://www.americanheart.org.

[2] Chatzizisis, Y. S. et al., Circ. **117** (2008) 993.

[3] Caro, C., Fitzgerald, J., and Schroter, R., Nature **223** (1969) 1159.

[4] Shaaban, A. M. and Duerinckx, A. J., AJR Am. J. Roentgenol. **174** (2000) 1657.

[5] Rybicki, F. J. et al., Intl. J. Cardiovasc. Imaging **24** (2008) 535.

[6] Steigner, M. L. et al., Intl. J. Cardiovasc. Imaging **25** (2009) 85.

[7] Succi, S., *The Lattice Boltzmann Equation for Fluid Dynamics and Beyond*, Oxford University Press, USA, 2001.

[8] Bernaschi, M. et al., Comp. Phys. Comm. **180** (2009) 1495.

[9] Benzi, R., Succi, S., and Vergassola, M., Phys. Rep. **222** (1992) 147.

[10] Boyd, J. and Buick, J. M., Phys. Med. Biol. **53** (2008) 5781.

[11] Ladd, A. J. C. and Verberg, R., J. Stat. Phys. **104** (2001) 1191.

[12] Guo, Z., Zheng, C., and Shi, B., Phys. Fluids **14** (2002) 2007.

[13] Mazzeo, M. and Coveney, P., Comp. Phys. Comm. **178** (2008) 894.

[14] Zou, Q. and He, X., Physics of Fluids **9** (1997) 1591.

[15] Latt, J., Chopard, B., Malaspinas, O., Deville, M., and Michler, A., Physical Review E **77** (2008) 056703.

[16] Melchionna, S. et al., Comput. Phys. Comm. **181** (2010) 462.

[17] Feldman, C. L. et al., Am. Heart J. **143** (2002) 931.